Control of electronic properties by lanthanide size and manganese oxidation state in the Mn^{III}/Mn^{IV} Ruddlesden–Popper phases $Ln_{2-x}Sr_{1+x}Mn_2O_7$

Peter D. Battle,* Mark A. Green, N. Scott Laskey, Nicholas Kasmir, Julie E. Millburn, Lauren E. Spring, Stuart P. Sullivan, Matthew J. Rosseinsky* and Jaap F. Vente

Inorganic Chemistry Laboratory, University of Oxford, South Parks Road, Oxford, UK OX1 3QR

The magnetic behaviour of the $n=2$ Ruddlesden–Popper phases $Sr_2LnMn_2O_7$ is very sensitive to the Ln^{3+} lanthanide cation. In samples with larger, more basic lanthanide cations (Ln = Nd, Pr) antiferromagnetic phases with ordering temperatures in the region of 130 K co-exist with phases showing a magnetic response suggestive of superparamagnetism or the development of small ferromagnetic clusters at high temperature. The magnetic transition temperature drops to 20 K in samples containing smaller, acidic cations (Ln = Gd–Er, Y). In the latter group of compounds, the transition is from a Curie–Weiss paramagnet to a spin-glass; there is no evidence for long-range magnetic order. This change in behaviour can be explained by considering the variation in the relative strength of superexchange and double exchange interactions as a function of the lanthanide cation. The influence of manganese oxidation state on magnetic response is investigated in the $Sr_{2-x}Ln_{1+x}Mn_2O_7$ composition range ($0.0 \leqslant x \leqslant 0.7$) for Ln = Nd, Tb.

Recently, considerable attention has been focused on the mixed-valent lanthanide manganate perovskites because of the marked dependence of their resistivity on applied magnetic fields.[1,2] The magnetoresistance, at a given temperature (T) and field (H), is defined as $MR(T,H)=\{[\rho(T,0)-\rho(T,H)]/\rho(T,H)\}\times 100$. The magnetoresistance in these systems is highly dependent on the size of the lanthanide cation, the manganese oxidation state and the temperature, and can be up to 10^{11} %, corresponding to almost 100% suppression of the zero-field resistance. The most common mechanism for this so-called 'colossal magnetoresistance' (CMR) is the occurrence of an insulator-to-metal transition accompanying the onset of ferromagnetism; application of fields of the order of 2–3 T at temperatures just above the Curie temperature (T_c) can drive the system into the metallic ferromagnetic state from the insulating paramagnetic state found in zero field, producing a very large resistance drop: a decrease of 2.5×10^7 % has been reported for $Sr_{0.05}Ca_{0.25}Pr_{0.7}MnO_{3-\delta}$ at 85 K in an applied field of 5 T.[3] T_c is strongly dependent on the cation size *e.g.* $T_c=380$ K for $La_{0.67}Sr_{0.33}MnO_3$ compared with $T_c=100$ K for $Sm_{0.67}Sr_{0.33}MnO_3$.[4] Large field-induced resistance changes also occur upon the melting of a 'charge-ordered' Mn^{III}/Mn^{IV} superlattice at the metamagnetic transition of antiferromagnets with equal concentrations of Mn^{III} and Mn^{IV} such as $Ca_{0.5}Pr_{0.5}MnO_3$.[5] Cation substitution at the A site has recently seen CMR observed in this class of material in fields as low as 0.4 T.[6]

The perovskite is the $n=\infty$ end-member of the $A_{n+1}B_nO_{3n+1}$ Ruddlesden–Popper family, in which n two-dimensional layers of BO_6 corner-sharing octahedra are joined along the stacking direction (z) with the neighbouring n-layer thick perovskite blocks being separated by rock-salt AO layers. The $n=1$ member is the two-dimensional K_2NiF_4 structure. $Sr_{1.2}La_{0.8}MnO_4$ with this structure is a spin-glass with a freezing temperature of 20 K and does not display CMR.[7] However, it has been demonstrated that the $n=2$ Ruddlesden–Popper phase $Sr_{1.8}La_{1.2}Mn_2O_7$[8] behaves in a similar manner to the simple $n=\infty$ perovskites: it undergoes a metal–insulator transition at its ferromagnetic Curie temperature[9] (126 K) and has a large magnetoresistance in this temperature region. The field required to induce this behaviour is, importantly, reduced to 0.3 T. The $Sr_{1.6}La_{1.4}Mn_2O_7$ phase is also ferromagnetic, with a reduced T_c of 90 K, and displays low-field CMR arising from suppression of domain boundaries in the insulating layers between the perovskite blocks.[10] The change in dimensionality apparently emphasises the cation dependence of the electronic properties and can produce physical properties which contrast strongly with the perovskite systems. Recently, it has been shown that colossal magnetoresistance in $Sr_{2-x}Nd_{1+x}Mn_2O_7$ is not associated with bulk three-dimensional ferromagnetic behaviour[11,12] and is therefore not readily explained by the double exchange mechanism, which has been used to account for the effect in those compounds where a loss of resistance has occurred close to a Curie point. High-resolution powder neutron diffraction measurements[13] indicate that the $x=0.0$ and $x=0.1$ members of this series exist as biphasic mixtures, with an antiferromagnetic phase and a phase without magnetic long-range order, considered to be either superparamagnetic or spin-glass-like. The former has (at $x=0.0$) a Neel temperature of 140 K for ordering of the Mn moments and 30 K for ordering of the Nd moments in the rock-salt layers. The lanthanide moments in the perovskite block do not produce magnetic Bragg scattering; they are either disordered and frozen, or paramagnetic in their behaviour at all temperatures.[13] Magnetisation measurements on $Sr_2NdMn_2O_7$ ($x=0.0$) and $Sr_{1.9}Nd_{1.1}Mn_2O_7$ ($x=0.1$) show the complexity expected for a biphasic mixture: $x=0.0$ has a susceptibility maximum at 210 K and a further local maximum at 140 K. The latter, but not the former, coincides with the appearance of magnetic Bragg scattering characteristic of antiferromagnetic order in the neutron diffraction pattern. The CMR onset is also below 140 K. At $x=0.1$ the Neel temperature for ordering of the manganese moments in the antiferromagnetic phase is reduced to about 100 K. The magnetoresistance of the $x=0.0$ and $x=0.1$ compositions is $>10^4$ % at 40 K in 14 T. Although recent work shows that grain boundary contributions to CMR are significant in ceramic samples at low fields over a wide temperature range,[14] the observation of CMR without bulk ferromagnetism is intriguing and requires explanation. Such an effect has been observed in only one other system, the $n=\infty$ perovskite $(Tb_{0.33}La_{0.67})_{0.67}Ca_{0.33}MnO_3$,[15,16] suggesting that further exploration of these $n=2$ Ruddlesden–Popper phases is warranted. The goal of this paper is to provide more detailed magnetic characterisation of a range of these materials.

Phase separation at the $Sr_2LnMn_2O_7$ composition is observed for all the phases Ln = La–Sm. Single-phase behaviour is found for Ln = Gd–Er, Y together with the ordering of the smaller Ln^{3+} cations onto the nine-coordinate rock-salt

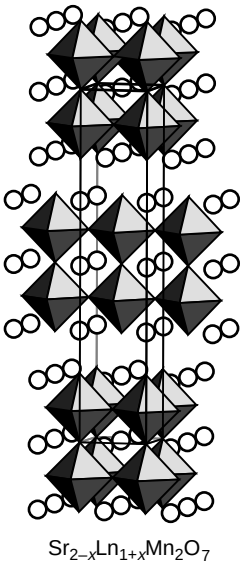

Fig. 1 The $n=2$ $(Ln_{1-x}Sr_x)_3Mn_2O_7$ Ruddlesden–Popper (RP) structure adopted by the phases discussed in the paper. MnO_6 octahedra are shaded. The nine-coordinate Ln/Sr site in the rocksalt layer and the twelve-coordinate site in the perovskite block are shown as circles.

layer A site;[17] the Sr^{2+} cations preferentially occupy the twelve-coordinate A site in the perovskite blocks. The structure is shown in Fig. 1. The *a* lattice parameter decreases to reach a minimum at the same point in the series where single phases form, while the unit-cell volume decreases monotonically with lanthanide size. We recently confirmed this picture of phase-separation at the 2:1 composition of $Sr_2NdMn_2O_7$ using synchrotron powder X-ray diffraction on samples prepared over a wide range of reaction temperatures (up to 1500 °C) and atmospheres.[18] The sensitivity of the product to precise synthesis conditions is demonstrated by our preparation of both single-phase and biphasic samples of the $Sr_2EuMn_2O_7$ composition, which allows a direct comparison of their behaviour. The aim of the present work is to see how the magnetic response associated with the unusual CMR in the Ln = Nd compounds changes with Ln^{3+} size (across the series $Sr_2LnMn_2O_7$) and on changing the manganese oxidation state and thus the number of electrons in the e_g orbitals. (The magnetic properties of the $La_{1-x}Ca_xMnO_3$ perovskites have been shown to depend strongly on the manganese oxidation state.[19]) In this paper the changes in magnetism on reduction towards Mn^{III} in $Sr_{2-x}Ln_{1+x}Mn_2O_7$ are investigated for phases with Ln = Nd, Tb. For $x \geqslant 0.4$ the Nd materials appear single phase to laboratory and synchrotron powder X-ray diffraction, whereas for Tb, compounds with $x \leqslant 0.5$ are single phase.

Experimental

The preparation and crystal chemistry of the majority of these materials is discussed in ref. 17. Magnetic measurements were carried out on $\approx$100 mg samples mounted in gelatin capsules using Quantum Design MPMS SQUID magnetometers for $5 \leqslant T/K \leqslant 300$ and $0.01 \leqslant \mu_0 H/T \leqslant 5$. Magnetisation isotherms at 300 K were used to test for possible ferromagnetic impurities. Isothermal remanent magnetisation (IRM) measurements were carried out on $Sr_2YMn_2O_7$ by cooling the sample from 60 K to 10 K in zero applied field, setting the field to a measuring value $\mu_0 H$ and then reducing it to zero and measuring the magnetisation (the IRM) in zero field.

The preparation of the single-phase sample of $Sr_2EuMn_2O_7$ involved the procedure discussed in ref. 17 but with an additional 36 h heating at 1350 °C. The lattice parameters of this phase are $a = 3.82912(7)$ Å and $c = 20.00443(46)$ Å. The lattice parameters differ from the phases in the biphasic sample in that *a* is slightly smaller than either of the two phases while *c* is slightly larger. The unit-cell volume of 293.31(2) Å.^{3} is very similar to that of the larger of the two phases found previously [293.28(2) Å^3]. $Sr_{1.3}Nd_{1.7}Mn_2O_7$ was prepared by firing stoichiometric quantities of $SrCO_3$, Nd_2O_3 and MnO_2 in air for 1 day at 800, 1000 and 1200 °C followed by five days at 1300 °C and 2 days at 1350 °C. The final reaction step was heating for 6 days at 1350 °C under flowing nitrogen. The lattice parameters of this phase are $a = 3.85406(7)$ Å, $c = 20.2992(4)$ Å.

The formal manganese oxidation state was determined by iodometric titration or oxidative back titration of Fe^{II} using dichromate for those samples which dissolved sufficiently rapidly to give reproducible results. Thermogravimetric reduction in flowing pure hydrogen below 1000 °C proved inconclusive as to the total oxygen concentration because the samples did not reduce completely.

Results

(*a*) $Sr_2LnMn_2O_7$ ($x = 0.0$)

Three distinct types of behaviour are apparent.

(i) $Sr_2NdMn_2O_7$, $Sr_2PrMn_2O_7$. Magnetisation measurements on $Sr_2NdMn_2O_7$ have been reported earlier[11] and do not show any sign of bulk ferromagnetism or metamagnetism in fields of up to 5 T, in contrast to what would be expected from a conventional CMR material. $M(H)$ measurements demonstrate that below the maximum in *M* at 212 K non-linearity and small amounts of hysteresis develop at 200 and 100 K, while $M(H)$ at 300 K is both non-hysteretic and linear. (Fig. 2).

Similar magnetisation in a 0.05 T field is observed for the $Sr_2PrMn_2O_7$ composition (Fig. 3), consistent with the observation of magnetoresistance in $Sr_{1.8}Pr_{1.2}Mn_2O_7$.[12] The FC and ZFC magnetisations increase dramatically below 270 K and then diverge in a manner reminiscent of the behaviour of $Sr_2NdMn_2O_7$. The maximum in *M* at 143 K suggests the onset of antiferromagnetic order in one of the two phases present by analogy with observations on $Sr_{2-x}Nd_{1+x}Mn_2O_7$.[11,13] The reduction of the ZFC magnetisation below 40 K signifies either spin-glass freezing or antiferromagnetic order of the Pr moments, by analogy with the behaviour of $Sr_2NdMn_2O_7$.

(ii) $Sr_2SmMn_2O_7$, $Sr_2EuMn_2O_7$. Magnetisation measurements on biphasic samples of both these materials (Fig. 4) show a sharp increase below 150 K, and do not display Curie–Weiss behaviour above this temperature. For $Sr_2SmMn_2O_7$, the ZFC magnetisation reaches a maximum at 29 K and the FC temperature dependence changes sign. For $Sr_2EuMn_2O_7$, the maximum in the ZFC magnetisation is at 21 K. The FC

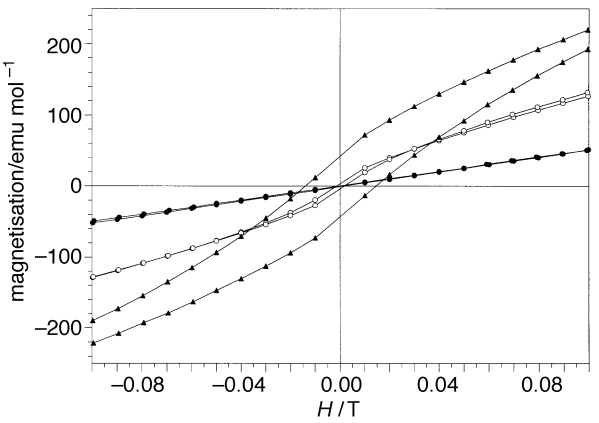

Fig. 2 Magnetisation as a function of field for $Sr_2NdMn_2O_7$ at 300 (●), 200 (○) and 100 K (▲), after cooling in a 5 T applied field

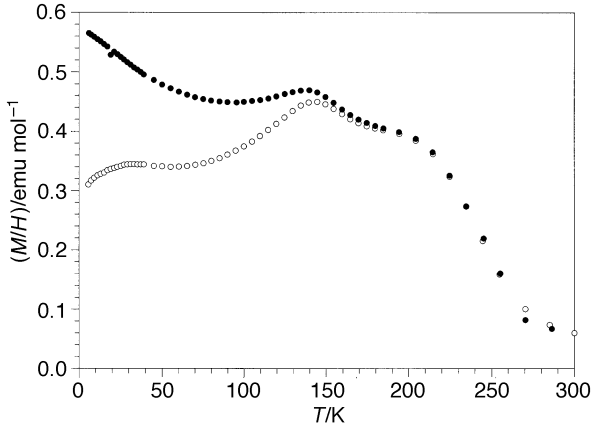

Fig. 3 Magnetisation of $Sr_2PrMn_2O_7$ measured in a 0.05 T field. Zero-field cooled (ZFC, open circles) and field cooled (FC, filled circles) data are shown.

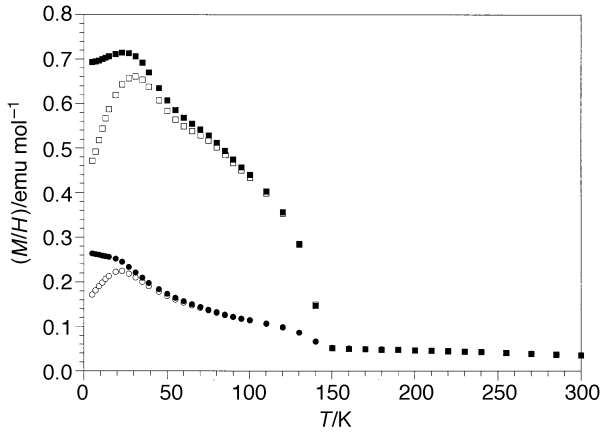

Fig. 4 Magnetisation of biphasic samples of $Sr_2EuMn_2O_7$ (●, FC; ○, ZFC) and $Sr_2SmMn_2O_7$ (■, FC; □, ZFC) in a field of 0.05 T, presented as in Fig. 2

magnetisation continues to increase with decreasing temperature but with a smaller gradient. At 180 K, $M(H)$ is linear for $Sr_2SmMn_2O_7$ [Figure 5(*a*)] but the linearity is lost below 150 K [Fig. 5(*a*) and (*b*)] and hysteresis effects are clearly apparent at 20 K. The centre of the hysteresis loop measured at 20 K is displaced slightly from the origin, while $M(H)$ measurements at 80 and 130 K are symmetric in shape [Fig. 5(*c*)].

The single-phase sample of $Sr_2EuMn_2O_7$ does not display the magnetisation jump at 150 K [Fig. 6(*a*)] but the spin-glass transition is retained, with T_F reduced from 21 K in the two-phase sample to 19 K in the single-phase case. This behaviour is similar to the monophasic samples formed by the smaller lanthanides discussed in (*iii*) below. The small jump in M at 150 K in the biphasic sample is thus a qualitatively new feature of an as-yet unidentified phase in the Sr–Sm–Mn–O and Sr–Eu–Mn–O phase diagram. The unit-cell volume of the single phase [293.31(2) Å^3] is similar to that of the 293.28(2) Å^3 phase in the biphasic sample, suggesting that the 150 K rise in the magnetisation is attributable to the phase with a unit cell volume of 293.18(3) Å^3. Fig. 6(*b*) shows a clearly displaced FC hysteresis loop characteristic of spin-glass behaviour in the monophasic sample.

(iii) $Sr_2LnMn_2O_7$, Ln = Gd–Er, Y. The magnetisation measurements made on the single-phase samples Ln = Gd–Er, Y for $5 \leqslant T/K \leqslant 300$ in a field of 0.05 T are presented in Fig. 7 and 8. The Weiss constants and the observed and calculated moments (on the basis of spin-only Mn^{III}, Mn^{IV} and a free-ion lanthanide contribution) are given in Table 1. All of these

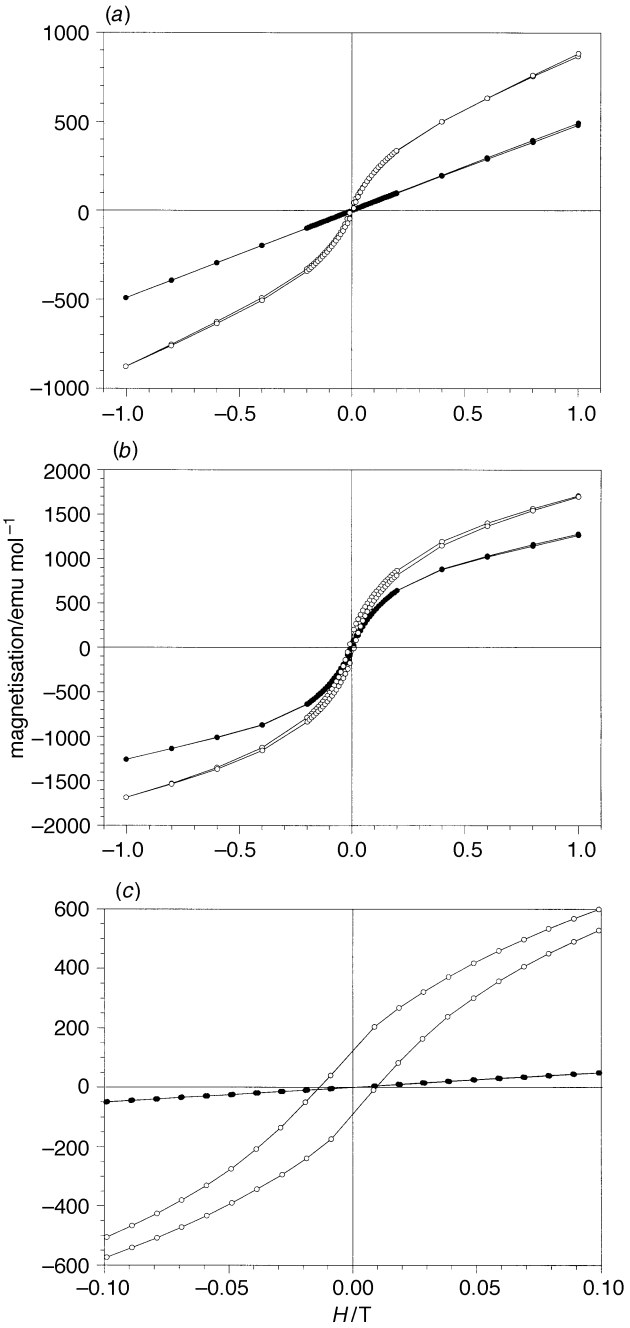

Fig. 5 $M(H)$ magnetisation loops measured on $Sr_2SmMn_2O_7$ after cooling in a 1 T field. (*a*) 180 (●) and 130 K (○), ±1 T; (*b*) 80 (●) and 20 K (○), ±1 T; (*c*) comparison of low-field measurements at 20 (○) and 180 K (●).

samples have similar behaviour, obeying the Curie–Weiss law reasonably well for $T \geqslant 100$ K (the phases with Ln = Gd, Y diverge from strict agreement below 240 K) with observed magnetic moments close to those expected on the basis of simple non-interacting ion models for the magnetism. Evidence for co-operative magnetic behaviour is apparent at lower temperatures in all of these samples. There is a small divergence between field-cooled (FC) and zero field-cooled (ZFC) magnetisation for all the samples where Ln^{3+} carries a paramagnetic moment, while a more marked divergence is apparent for $Sr_2YMn_2O_7$: the freezing transition of the latter compound is shown in more detail in a 0.01 T measuring field in Fig. 8(*b*). The variation of the freezing temperature, T_F, with the lanthanide in a 0.05 T measuring field is given in Table 1.

To investigate the low-temperature behaviour of the $Sr_2YMn_2O_7$ phase, we carried out 1 T FC magnetisation

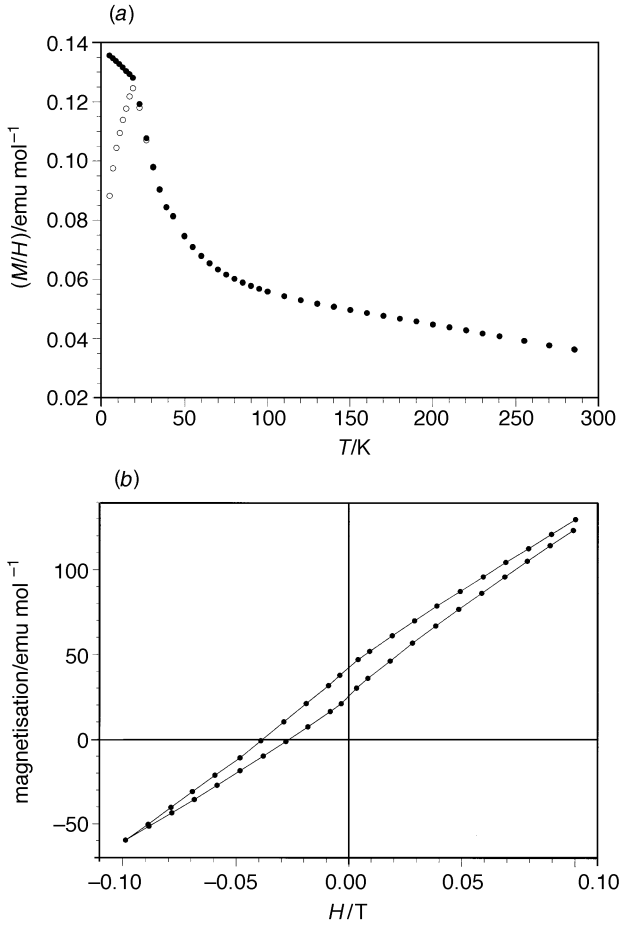

Fig. 6 (*a*) Magnetisation of a single-phase sample of $Sr_2EuMn_2O_7$ measured in a 0.05 T field (○, ZFC; ●, FC). (*b*) $M(H)$ magnetisation loops measured on a single-phase sample of $Sr_2EuMn_2O_7$ after cooling in a 0.1 T field at 5 K.

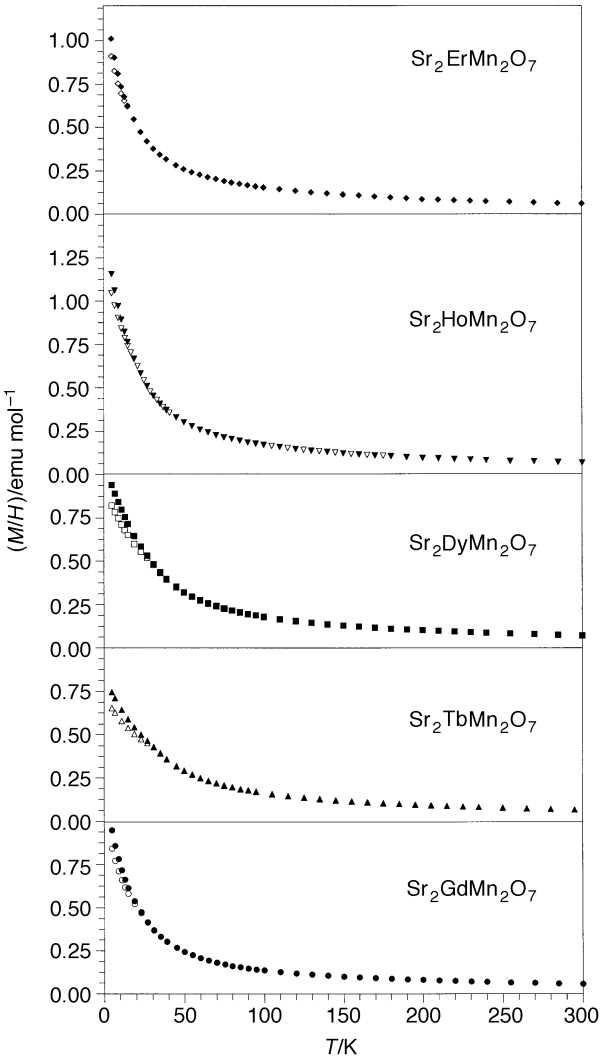

Fig. 7 Magnetisation of single-phase samples of $Sr_2LnMn_2O_7$ (Ln = Gd–Er) measured in a 0.05 T field (empty symbols, ZFC; filled symbols, FC)

isotherm and isothermal remanent magnetisation (IRM) measurements. The measurements shown in Fig. 9 indicate that there is neither hysteresis nor non-linearity in $M(H)$ at 100 K, (in contrast with, for example, $Sr_2NdMn_2O_7$) whereas at 10 K hysteresis is observed. The IRM at 10 K saturates in a field of 1.2 T. (Fig. 10). $M(H)$ isotherms measured in fields of up to 5 T after zero-field cooling indicate the absence of any metamagnetic transitions similar to those found for charge-ordered $n = \infty$ perovskites in this manganese oxidation state range, although $M(H)$ becomes significantly non-linear below T_F (Fig. 11). A 1 T FC $M(H)$ loop for $Sr_2HoMn_2O_7$ at 5 K (Fig. 12) also shows hysteresis, with a small displacement of the centre of the loop from the origin again visible.

(*b*) $Sr_{2-x}Tb_{1+x}Mn_2O_7$

Iodometric titration proved suitable for a reliable determination of the manganese oxidation states in this series, and the resulting oxidation states are shown in Table 2 along with the oxygen concentrations derived from the assumption that there are no cation vacancies in the structure which might also control the deviations from the expected oxidation state. Phases prepared under air and oxygen incorporate small quantities of excess oxygen (presumably located in the rock-salt layers), whereas the more reduced samples prepared under nitrogen have small oxygen deficiencies. The trend in the oxidation states mirrors that expected from the change in Sr/Tb ratio *i.e.* increasing x corresponds to increasing filling of the e_g band.

The magnetisation curves of all these materials (Fig. 13) show a smooth increase on cooling from 300 K to about 40 K. The Curie–Weiss law applies well over a wide temperature range for the single-phase $x = 0.0$, 0.1 and 0.3 compositions,

Table 1 Magnetic properties of single-phase $Sr_2LnMn_2O_7$ samples. The freezing temperature, T_F, is defined as the temperature at which the ZFC and FC magnetisations reach their maxima.

compound	Curie–Weiss range/K	μ_{calc}/μ_B	μ_{obs}/μ_B	θ/K	T_F/K (0.05 T)
$Sr_2GdMn_2O_7$	240–300	10.1	11.8(3)	−9(3)	19
$Sr_2TbMn_2O_7$	100–300	11.6	13.3(1)	−35.8(8)	27
$Sr_2DyMn_2O_7$	100–300	12.3	13.8(4)	−36.2(7)	27
$Sr_2HoMn_2O_7$	100–300	12.3	13.40(5)	−33.4(6)	15
$Sr_2ErMn_2O_7$	100–300	11.4	12.7(1)	−30(1)	13
$Sr_2YMn_2O_7$	240–300	4.9	6.6(2)	+8(5)	17

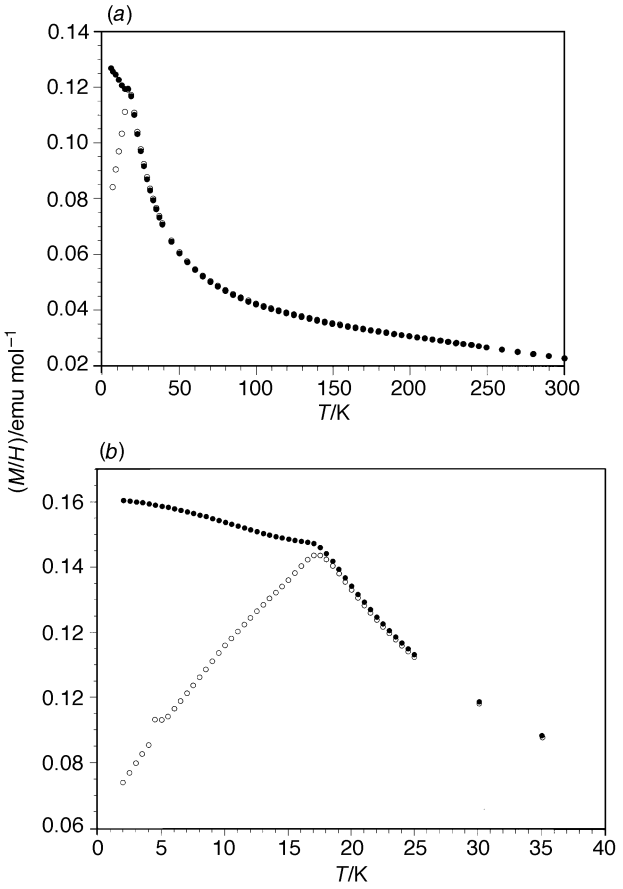

Fig. 8 (*a*) Magnetisation of single-phase $Sr_2YMn_2O_7$ measured in a 0.05 T field. (*b*) Freezing transition of the spin-glass $Sr_2YMn_2O_7$ in a measuring field of 0.01 T (○, ZFC; ●, FC).

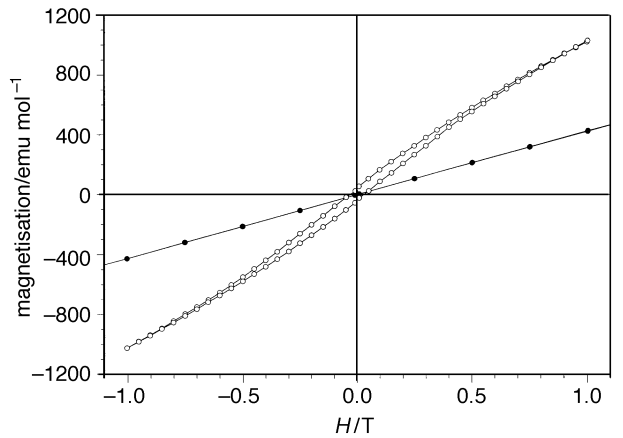

Fig. 9 $M(H)$ magnetisation loops measured on $Sr_2YMn_2O_7$ after field cooling at 100 K (●, 5 T cooling field) and 10 K (○, 1 T cooling field)

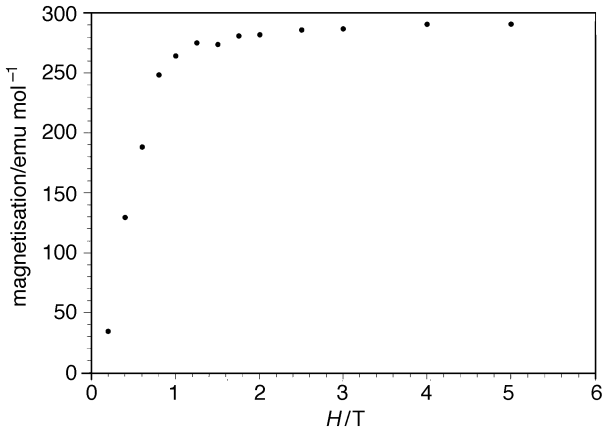

Fig. 10 Isothermal remanent magnetisation of $Sr_2YMn_2O_7$ at 10 K

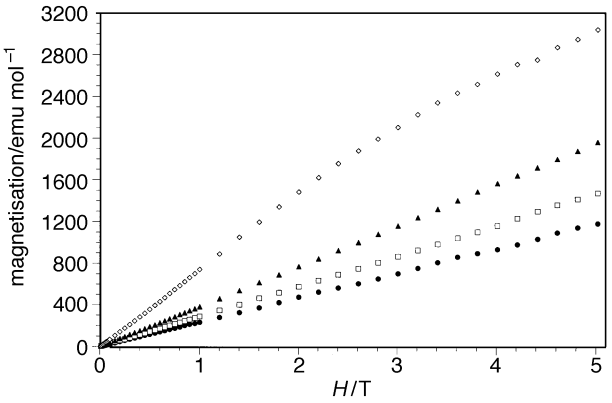

Fig. 11 $M(H)$ ZFC magnetisation isotherms of $Sr_2YMn_2O_7$ at 5 (◇), 100 (▲), 200 (□) and 300 K (●)

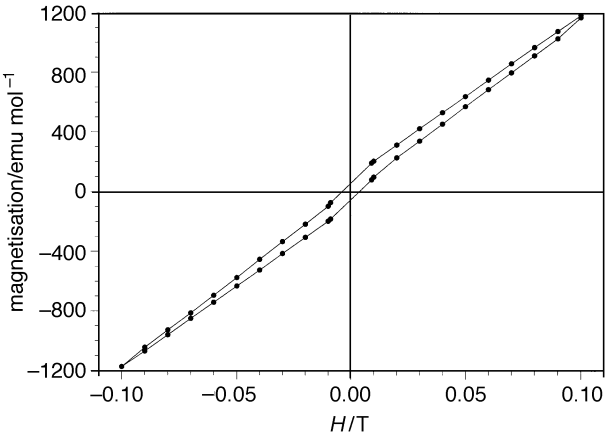

Fig. 12 $M(H)$ magnetisation loops measured on $Sr_2HoMn_2O_7$ at 5 K after cooling in a 0.1 T field

although the moments are larger than calculated using a simple non-interacting electron model (Table 3). The Weiss constant changes sign to become positive at the biphasic $x=0.5$ composition, which also has the highest freezing temperature (defined as the temperature where the FC and ZFC magnetisations diverge). At low temperatures, the divergence between FC and ZFC magnetisation occurs in a similar way to the $x=0$ phase.

(*c*) $Sr_{2-x}Nd_{1+x}Mn_2O_7$

The manganese oxidation states and oxygen concentrations (derived on the assumption that there are no manganese or A site vacancies; these defects are in fact the main charge-compensation mechanism in the $n=\infty$ end-member[20]) resulting from iodometric titrations on this series are given in Table 4. All the samples are stoichiometric or display a slight oxygen excess. The only point in the series where the oxidation state evolution does not follow that expected on the basis of the Sr/Nd ratio is between $x=0.1$ and 0.2. These two compounds have the same mean Mn oxidation state within experimental error, although the significantly different magnetisation behaviour does suggest a slight difference in the concentration of electrons in the e_g orbitals.

The magnetisation measurements on these samples are shown in Fig. 14(*a*). The $x=0.2$ and 0.3 samples have magnetisation curves which qualitatively resemble that for $x=0.1$ reported previously.[11] In view of the unusual nature of the

Table 2 Manganese oxidation state in $Sr_{2-x}Tb_{1+x}Mn_2O_y$ determined by iodometric titration. The expected oxidation state is calculated on the basis of a composition $Sr_{2-x}Tb_{1+x}Mn_2O_7$.

x in $Sr_{2-x}Tb_{1+x}Mn_2O_y$	expected Mn oxidation state	measured Mn oxidation state	y in $Sr_{2-x}Tb_{1+x}Mn_2O_y$
−0.1	3.55	3.59(1)	7.04
0.0	3.50	3.56(1)	7.06
0.1	3.45	3.30(1)	6.85
0.3	3.35	3.22(1)	6.87
0.5	3.25	3.20(1)	6.95

Table 3 Magnetic properties of $Sr_{2-x}Tb_{1+x}Mn_2O_y$. The freezing temperature is defined as in Table 1.

compound	Curie–Weiss range/K	μ_{calc}/μ_B	μ_{obs}/μ_B	θ/K	T_F/K (0.05 T)
$Sr_2TbMn_2O_7$	100–300	11.6	13.3(1)	−35.8(8)	27.0
$Sr_{1.9}Tb_{1.1}Mn_2O_7$	120–300	12.0	17.7(3)	−53(1)	23
$Sr_{1.7}Tb_{1.3}Mn_2O_7$	80–300	12.8	14.1(1)	−14.3(8)	31
$Sr_{1.5}Tb_{1.5}Mn_2O_7$	240–300	13.6	12.2(3)	86.3(3)	37

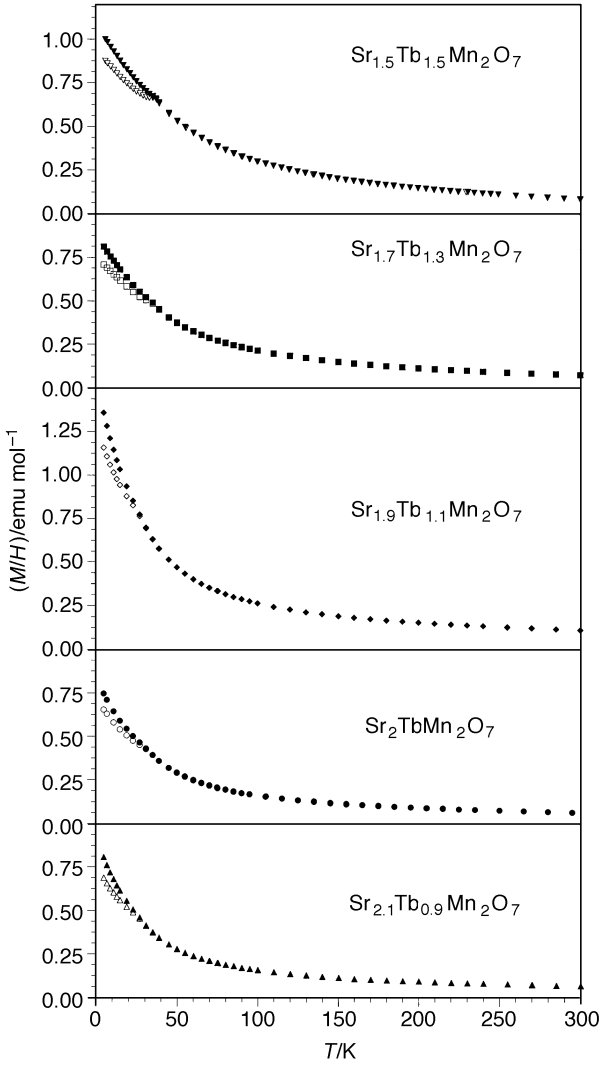

Fig. 13 Magnetisation of $Sr_{2-x}Tb_{1+x}Mn_2O_7$ measured in a 0.05 T field. FC measurements are shown as filled symbols, ZFC as empty symbols.

observation of CMR without bulk ferromagnetism in $Sr_{2-x}Nd_{1+x}Mn_2O_7$, we carefully investigated the field dependence of the magnetism over a wide temperature range for the samples with $x=0.1$ and 0.2. The $M(H)$ loops in Fig. 15, measured on field cooling from 300 K to the measuring temperature, show that very small quantities of hysteresis are observed below the temperature at which the susceptibility shows a marked increase. The area enclosed by the hysteresis loops increases on cooling in all cases. No remanent moment is measurable because the coercive field is <0.01 T. Extrapolation of the linear part of the data to zero field yields 0.24 μ_B/Mn and 0.56 μ_B/Mn for $x=0.1$ and $x=0.2$ at 5 K. Comparison of the magnetic properties of an $x=0.2$ sample prepared by our subsolidus route with that prepared by a recently presented method involving a Bi_2O_3 flux indicates that their magnetic properties are similar but differ in detail. The temperature of the sharp rise in the magnetisation is constant at 280 K but the extrapolated zero-field moment at 5 K is 0.51 μ_B/Mn in the flux sample and 0.56 μ_B/Mn from the solid-state reaction. The significance of this number is such a complex system is unclear and model-dependent. Fig. 16 shows the temperature region around the sharp rise in the magnetisation of $Sr_{1.8}Nd_{1.2}Mn_2O_7$ measured in two different fields. The transition is broadened in the 1.45 T field.

The single-phase samples with $x \geqslant 0.4$ do not have an abrupt rise in the magnetisation below 300 K. They display susceptibility maxima and hysteresis at lower temperatures, the onset temperature of hysteresis increasing with decreasing measuring field for $x=0.7$ (Fig. 17). When compared with the $Sr_{2-x}Tb_{1+x}Mn_2O_7$ series, the Curie–Weiss law has very limited applicability. The single phase samples with $x=0.4$ and 0.7 do have Curie–Weiss behaviour at higher temperatures (above 200 K), and, interestingly, both have positive Weiss constants in the range of *ca.* 100 K. The observed magnetic moments are about 1 μ_B higher than the simple theoretical values. (Table 5). For all the $Sr_{2-x}Nd_{1+x}Mn_2O_7$ series, the effective moment $(8\chi T)^{1/2}$ evaluated at 300 K is also in excess of the non-interacting ion value.

Hysteresis in the single-phase samples begins at a temperature T_d, which is greater than the temperature of the maximum in the magnetisation, T_F. This is consistent with competing interactions producing blocked clusters of spins[21] prior to the freezing of the magnetically frustrated system which occurs at approximately 50 K in a 0.05 T measuring field. Other interpretations of this behaviour are possible and are given in the discussion section. The temperatures T_d and T_F in a 0.05 T measuring field are given in Table 5, and the magnetisation in the vicinity of T_d is shown for $Sr_{1.6}Nd_{1.4}Mn_2O_7$ in Fig. 14(*b*). The $x=0.7$ sample shows hysteresis after field cooling in 1 T to 5 K (Fig. 18). These observations are also consistent with the development of small clusters of correlated spins with net ferromagnetic moments as well as canonical spin-glass behaviour.

Table 4 Manganese oxidation state in $Sr_{2-x}Nd_{1+x}Mn_2O_y$ determined by iodometric titration. The expected oxidation state is calculated on the basis of a composition $Sr_{2-x}Nd_{1+x}Mn_2O_7$.

x in $Sr_{2-x}Nd_{1+x}Mn_2O_y$	expected Mn oxidation state	measured Mn oxidation state	y in $Sr_{2-x}Nd_{1+x}Mn_2O_y$
0.0	3.50	3.54(1)	7.04
0.1	3.45	3.46(1)	7.01
0.2	3.40	3.47(1)	7.07
0.3	3.35	3.40(1)	7.05
0.5	3.25	3.26(1)	7.01
0.7	3.15	3.15(1)	7.00

Table 5 Magnetic properties of $Sr_{2-x}Nd_{1+x}Mn_2O_7$. The divergence and freezing temperatures, T_d and T_F are defined in the text.

x in $Sr_{2-x}Nd_{1+x}Mn_2O_7$	Curie–Weiss range/K	μ_{calc}/μ_B	μ_{obs}/μ_B	θ/K	T_d/K (0.05 T)	T_F/K (0.05 T)
0.4	220–300	7.8	9.11(9)	82(1)	130	45
0.5	—	—	—	—	180	50
0.7[a]	220–300	8.2	9.8(1)	88(1)	65	45

[a]For $x=0.7$, $T_F=50$ K $T_d=120$ K in a lower measuring field of 0.01 T.

Discussion

We begin our discussion by summarising the electronic structure and behaviour of the more widely studied ABO_3 $n=\infty$ perovskites, to establish energy scales and types of interaction which will be relevant in the $n=2$ phases which are the subject of the present paper. The parent $La_{1-y}Mn_{1-x}O_3$ perovskite, when prepared with the Mn^{III} oxidation state, is an antiferromagnetic insulator with a Neel temperature of 100 K and an ordered Jahn–Teller distortion of the MnO_6 octahedra.[22] Recent LDA+U calculations suggest that the gap is of the charge-transfer (O_{2p}–Mn_{3d}) insulator rather than the Mott–Hubbard (3d–3d) type.[23] The electronic configuration of the Mn^{III} cation ($t_{2g}^3e_g^1$) comprises two distinct classes of electrons. The t_{2g}^3 electrons are considered, in the double exchange treatment, to be localised spins ($S=3/2$) because of the weak π-symmetry hybridisation with the O (2p) states, although it is interesting to note that the calculations referred to above give them a bandwidth similar to that of the e_g states. In contrast, the strong hybridisation of the σ^* e_g^1 states with oxygen is assumed to produce a broader band. The σ^* electrons are localised in the Mn^{III} parent system, because of the influence of the Hubbard U when the ratio of electrons to available sites is one: theoretical[23] and experimental[24] estimates of U are in the range of 4–5 eV. Introduction of σ^* holes by partial oxidation to Mn^{IV} allows the e_g electrons to become itinerant if the bandwidth is sufficient to overcome the polaronic charge fluctuation energy of 1.5 eV.[24] The delocalised holes exert a strong influence on the magnetism, and introduce the metal–insulator transition accompanied by the onset of ferromagnetism which has come to be seen as the hallmark of CMR materials. This has been interpreted in terms of ferromagnetic double exchange interactions which compete with the antiferromagnetic π-symmetry superexchange. The latter is the dominant interaction when the e_g orbitals are half-occupied and the electrons are consequently localised. The combined influence of the competing magnetic interactions and the polaronic 'charge-ordering' effects outlined in the introductory section make the electronic phase diagrams of the $A_xLn_{1-x}MnO_3$ perovskites (where A is an alkaline earth cation) complex and highly dependent on the nature of both the Ln^{3+} and A^{2+} cations.[5]

It is simplest to begin with consideration of the $Sr_2LnMn_2O_7$ single-phase samples (Ln=Tb–Er, Y). In these phases, the lanthanide cations are predominantly ordered on the nine-coordinate sites in the rock-salt layers of the structure, and the a parameter has reached its minimum value.[17] In contrast to Ln=La, Pr, Nd the $n=2$ RP phase does not display CMR for these cations.[25] The magnetisation measurements presented here on the two sets of phases (CMR and non-CMR) clearly show that their electronic properties are different. The single-phase small lanthanide compounds obey the Curie–Weiss law above 100 K and only display co-operative magnetism at lower temperature, signalled for the samples containing a paramagnetic lanthanide by a slight divergence between the FC and ZFC magnetisation. Clearer insight into the origin of this behaviour is provided by the behaviour of $Sr_2YMn_2O_7$ because the absence of a lanthanide magnetic moment allows us to investigate the response of the manganese spin system in a single-phase sample with an average manganese oxidation state of +3.5.

Extensive experiments on the $n=\infty$ three-dimensional perovskites with this oxidation state indicate that the competition between ferromagnetic (FM) and antiferromagnetic (AFM) interactions is very strong. For example, while $La_{1-x}Sr_xMnO_3$ retains its transition to ferromagnetic order as the oxidation state increases to beyond +3.5,[26] the $n=1$ system $La_{0.5}Sr_{1.5}MnO_4$ undergoes charge ordering of the +III and +IV valences in real space at 220 K followed by antiferromagnetic ordering at 120 K.[27] Changing the cation to the smaller, more electronegative Ca^{2+} results in $La_{0.5}Ca_{0.5}MnO_3$ undergoing a transition between two different magnetically ordered states driven by the localisation of charge at distinct +III and +IV sites in an ordered manner. After initially ordering ferromagnetically at 200 K, the onset of charge-ordering at 160 K produces a change to antiferromagnetic order.[19,28] The charge ordered state persists over a wider oxidation state range in $Pr_{1-x}Ca_xMnO_3$. ($x=0.3$–0.5). The reduced width of the Mn 3d band, ascribed to increased tilting of the MnO_6 octahedra,[29] clearly favours the charge-localised state. Reducing n, the number of contiguous blocks shared along the z direction, will also reduce the bandwidth and both favour charge ordering and increase the relative importance of the Hubbard U.

The measurements on $Sr_2YMn_2O_7$ should then be viewed in the context of the strong competition between FM and AFM exchange interactions at the +3.5 formal oxidation state and the influence of both dimensionality and the Mn 3d bandwidth on the tendency for charge ordering often associated with antiferromagnetism. The charge-ordering transition in $Sr_{0.5}La_{1.5}MnO_4$ is signalled in the susceptibility by a maximum at 250 K, with a small rise at the Neel temperature of 210 K,[27] while the magnetisation of $La_{0.5}Ca_{0.5}MnO_3$ drops sharply at its coincident charge and antiferromagnetic ordering temperatures.[28] $Sr_2YMn_2O_7$, by contrast, does not show the signature of antiferromagnetic ordering in the temperature range 5–300 K. Magnetisation measurements in 0.05 and 0.01 T fields

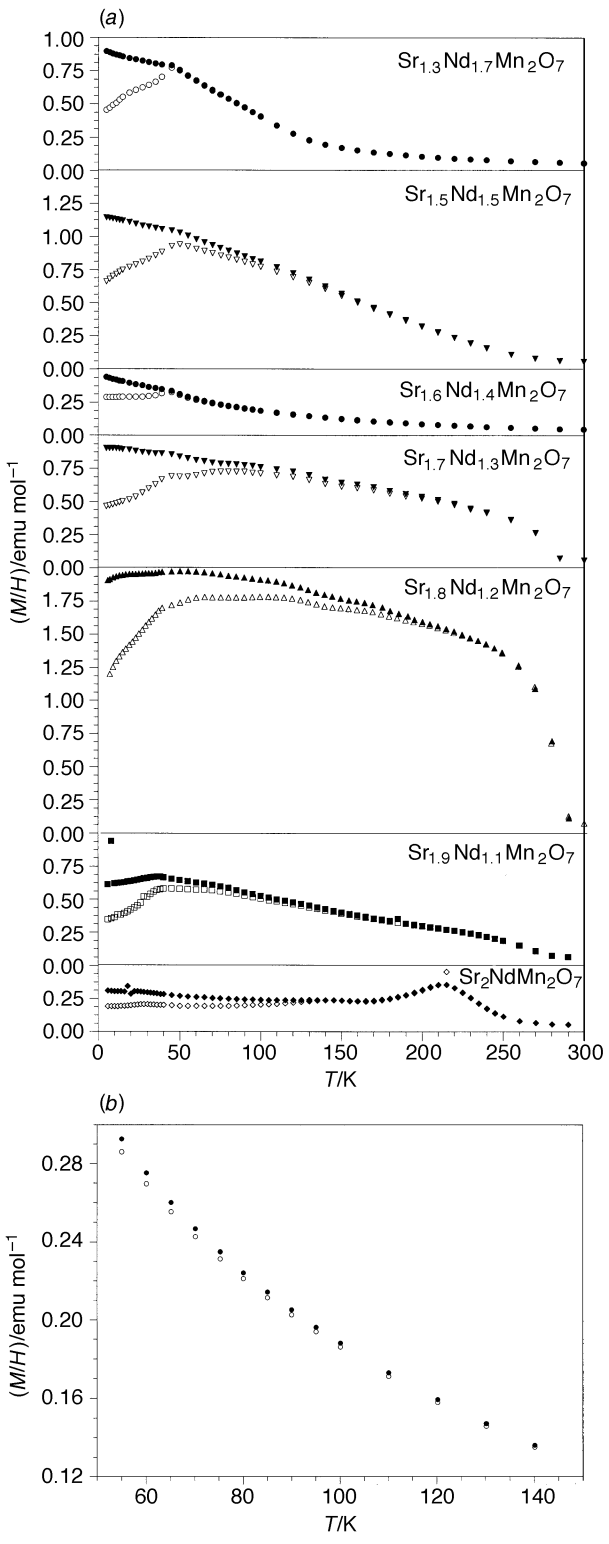

Fig. 14 (*a*) Magnetisation of $Sr_{2-x}Nd_{1+x}Mn_2O_7$ measured in a 0.05 T field. FC measurements are shown as filled symbols, ZFC as empty symbols. (*b*) Magnetisation of $Sr_{1.6}Nd_{1.4}Mn_2O_7$ measured in a 0.05 T field between 50 K and 150 K, showing the divergence between FC (●) and ZFC (○) magnetisation.

are characteristic of spin-glass behaviour (the FC magnetisation is temperature independent below the freezing temperature T_F whereas the ZFC magnetisation drops with decreasing temperature) with a T_F of 16 K. $M(H)$ is linear and non-hysteretic above 16 K. The observation of hysteresis below this temperature, together with isothermal remanent magnetisation saturating at a field of 1.2 T is consistent with spin-glass behaviour in this material, which is confirmed by the absence

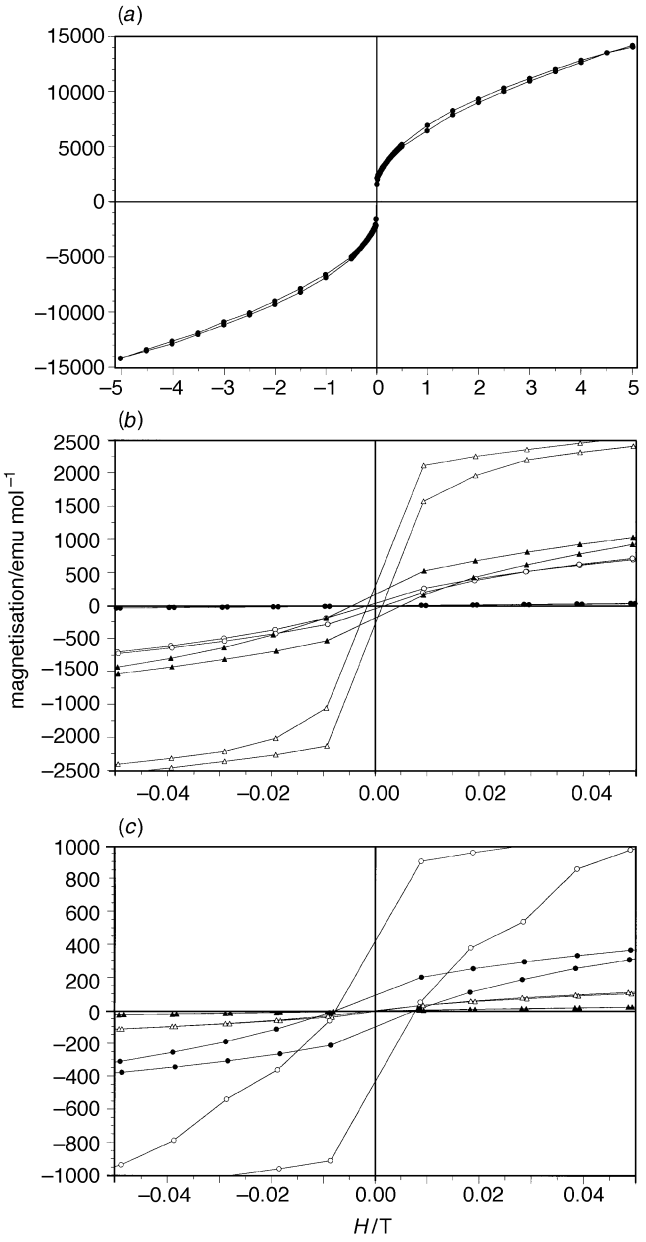

Fig. 15 (*a*) FC $M(H)$ measurement of $Sr_{1.8}Nd_{1.2}Mn_2O_7$ at 5 K, ±5 T, ±5 T. (*b*) Low-field part of $M(H)$ measurements on $Sr_{1.8}Nd_{1.2}Mn_2O_7$ at 5 (△), 100 (▲), 250 (○) and 300 K (●). (*c*) Low-field part of $M(H)$ measurements on $Sr_{1.9}Nd_{1.1}Mn_2O_7$ at 5 (○), 70 (●), 250 (△) and 300 K (▲).

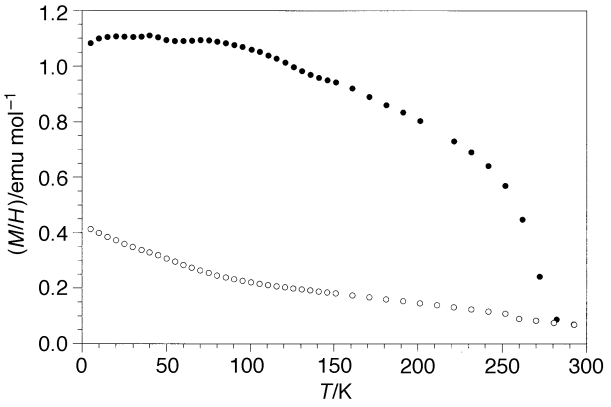

Fig. 16 Magnetisation as a function of temperature measured on $Sr_{1.8}Nd_{1.2}Mn_2O_7$ prepared in a Bi_2O_3 flux[12] in 0.05 (●) and 1.45 T (○) measuring fields. Data were collected after cooling in the measuring field.

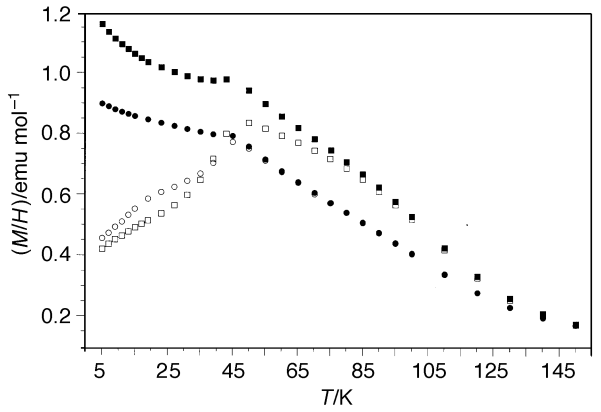

Fig. 17 Magnetisation of $Sr_{1.3}Nd_{1.7}Mn_2O_7$ measured in 0.05 (○, ●) and 0.01 T (□, ■) fields. FC data are filled symbols, ZFC data are empty symbols.

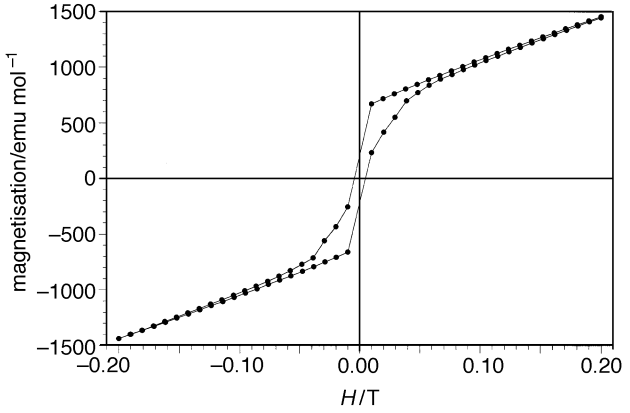

Fig. 18 $M(H)$ loop measured on $Sr_{1.3}Nd_{1.7}Mn_2O_7$ after field cooling in 0.2 T at 5 K

of magnetic Bragg peaks in the neutron powder diffraction pattern at 1.5 K.[30] We therefore assign the divergence of the FC and ZFC magnetisations at low temperature (below 20 K) for all the single-phase $Sr_2LnMn_2O_7$ samples Ln = Gd–Er, Y to spin-glass freezing of the manganese moments. The divergence of the FC and ZFC magnetisation for the paramagnetic lanthanide phases is less marked than for $Sr_2YMn_2O_7$. This, together with the similarity of the freezing temperatures, suggests that the freezing involves only the manganese spin system, with the lanthanide moments remaining essentially uncoupled to the transition metal ones and responding as simple paramagnets. Hysteresis is observed at 5 K in $M(H)$ measurements on $Sr_2HoMn_2O_7$, consistent with the assignment of the divergence in the susceptibility to spin-glass behaviour for the paramagnetic lanthanides as well as $Sr_2YMn_2O_7$. It should be noted that the two-dimensional square lattice is not geometrically frustrated, and the spin-glass freezing must arise because of competing interactions (discussed below) and disorder in the spatial location of Mn^{III} and Mn^{IV}, combined with the Sr/Ln disorder on the rock-salt layer site. Above the freezing temperature of $Sr_2YMn_2O_7$, the size and temperature dependence of the susceptibility is consistent with strong frustration of any antiferromagnetic exchange interactions, and with the presence of small clusters of aligned spins, as the Weiss constant is slightly positive and the observed Bohr magneton number is higher than that calculated on the basis of localised non-interacting ions.

The absence of CMR in $Sr_2YMn_2O_7$ together with the applicability of the Curie–Weiss law at high temperatures leads us to propose that the e_g electrons are localised in this compound over the 5–300 K temperature range. The localised e_g electrons will interact *via* superexchange with each other and the localised t_{2g} moments. The t_{2g}–t_{2g} interaction is antiferromagnetic (AF), while the t_{2g}–e_g superexchange interaction is ferromagnetic (F). The sign of the local e_g–e_g superexchange between two Mn^{III} centres depends critically on the existence of a Jahn–Teller distortion and the nature of any co-operative orbital ordering: both AF and F interactions are possible. Spin-glass behaviour could then arise from disorder of the localised +III and +IV oxidation states together with the competing F and AF interactions. These strong competing interactions account for the deviations from the Curie–Weiss law. Commensurate charge order would, by analogy with the $n=1$ and $n=\infty$ systems, produce an ordered antiferromagnetic ground state, and so charge localisation here would be either disordered or incommensurate.

The lanthanide magnetic moments in the single-phase materials also behave differently from the neodymium spins in the $x=0.0$ and 0.1 members of the $Sr_{2-x}Nd_{1+x}Mn_2O_7$ series. The increase in both FC and ZFC magnetisation below T_F(Mn) is in contrast to that observed for $Sr_2NdMn_2O_7$ below 140 K[11] and indicates a qualitative difference in coupling between the lanthanide and manganese moments as the size of the Ln^{3+} cations decreases. It is important to remember that the preferential occupancy of the nine co-ordinate rock-salt layer site increases as the Ln^{3+} cations get smaller from Nd to Er.[17] The Nd^{3+} ordering and freezing temperatures of 30 K observed in $Sr_2NdMn_2O_7$ are high and suggest strong coupling with the Mn spins.[13] The absence of lanthanide freezing or ordering above 5 K when the Ln^{3+} cation is Gd^{3+} or smaller indicates that the suppression of the high-temperature ordering and freezing of the manganese moments similarly reduces the manganese–lanthanide coupling, with the residual lanthanide–lanthanide interactions being insufficient to produce ordering.

The biphasic $Sr_2EuMn_2O_7$ and $Sr_2SmMn_2O_7$ samples behave similarly but differ from the two ends of the lanthanide series. The absence of Curie–Weiss behaviour at any point is partly due to the temperature dependence expected for the magnetic moments of these two lanthanide cations. A rise in the magnetisation of both of the biphasic samples studied here occurs below 150 K, followed by a divergence between the FC and ZFC magnetisation measured in 0.05 T below 100 K and a change in the sign of the temperature dependence of the ZFC magnetisation below 20 K, which may be associated with a freezing of the Mn moments as found for the single-phase samples of the later lanthanides. The 150 K jump is associated with the onset of hysteresis in the $M(H)$ measurements, and is therefore qualitatively similar to the more pronounced high-temperature steps found for the larger lanthanides. It may arise from a small canting associated with antiferromagnetic long-range order of the manganese moments (recall T_N is 137 K for the antiferromagnetic phase in $Sr_2NdMn_2O_7$[13]) or from the development of the superparamagnetic or small ferromagnetic clusters discussed below in the $Sr_{2-x}Nd_{1+x}Mn_2O_7$ series in connection with the jump in M just below 300 K. The behaviour of the single-phase $Sr_2EuMn_2O_7$ sample prepared under slightly different synthetic conditions confirms the picture of a low-temperature spin-glass phase ($T_F=21$ K) and a second phase with a higher energy scale for co-operative magnetism: it is the former which we have now prepared as a pure phase. The higher temperature (150 K) hysteresis found for the Sm case can then, by analogy, be ascribed to a phase other than that responsible for the low-temperature freezing. The absence of a rise in the FC or ZFC magnetisations below T_F in this case indicates that the Eu^{3+} cations are predominantly in the $J=0$ level in this temperature range or freeze together with the manganese spins. This point could be resolved by Mössbauer spectroscopy experiments. The Sm^{3+} cation does not have a non-magnetic ground state and therefore must be freezing or ordering at this temperature.

Considering the $Sr_2PrMn_2O_7$ system, which is both biphasic and displays CMR, analogy with the biphasic Nd system[13]

suggests that antiferromagnetic order occurs in one phase at 150 K, where the magnetisation reaches a local maximum. The formation of small clusters of correlated spins produces the rise in the magnetisation below 270 K: as in the $Sr_{2-x}Nd_{1+x}Mn_2O_7$ case it is impossible to tell which phase this arises in. We therefore suggest that the two phases present in the Ln = Pr sample behave similarly to the Nd case, *i.e.* there is one antiferromagnetic phase and a phase which displays high-temperature co-operative magnetic effects without long-range order, ascribable to the development of clusters of correlated spins.

It is for the larger lanthanides La^{3+}, Nd^{3+} and Pr^{3+} that CMR and the high-temperature irreversibility in magnetic response which appears to accompany it are to be found. The $Sr_{2-x}La_{1+x}Mn_2O_7$ Ruddlesden–Popper phases have the closest resemblance in crystal chemistry and electronic behaviour to the CMR $n=\infty$ perovskites. Phases with $x=0.2$ and 0.4 show three-dimensional ferromagnetic ordering,[8,10] while $x=0.0$ is a biphasic mixture of the $x=0.2$ ferromagnet and an antiferromagnet with a manganese oxidation state slightly higher than +3.5.[31] The three-dimensional ferromagnets $La_{1.6}Sr_{1.4}Mn_2O_7$[10] and $La_{1.8}Sr_{1.2}Mn_2O_7$[32] show deviations from the Curie–Weiss law at 240 and 280 K respectively, assigned to the development of two-dimensional ferromagnetic correlations within the bilayers. The metallic behaviour and three-dimensional ferromagnetic ordering observed in the $Sr_{2-x}La_{1+x}Mn_2O_7$ series does not survive as the lanthanide size is reduced, as shown by the electronic properties of the $Sr_{2-x}Tb_{1+x}Mn_2O_7$ and $Sr_{2-x}Nd_{1+x}Mn_2O_7$ series. These systems were chosen as they allow investigation of the effect of changing the manganese oxidation state on the magnetic properties in the two distinct classes of $Sr_2LnMn_2O_7$ phases ($Ln \neq La$) revealed thus far.

The change in the manganese oxidation state across the terbium series with increasing x mirrors that expected, and for simplicity we refer to nominal oxygen concentrations in the following discussion. Reducing the manganese oxidation state to below +3.5 from the single-phase spin-glass $Sr_2TbMn_2O_7$ produces a slight variation in the freezing temperature ($x=0.1$, 23 K; $x=0.3$, 31 K; $x=0.5$, 37 K), but the magnetisation measurements indicate that the basic physics of 'small lanthanide' $n=2$ RP phases is preserved despite the increase in the number of e_g electrons which produces the change from antiferromagnetism to ferromagnetism in the $Sr_{2-x}La_{1+x}Mn_2O_7$ series. In the Tb case, the low-temperature freezing of the Mn moments is preserved while the Tb moments retain their paramagnetic character. The transition to multiple phase behaviour observed beyond $x=0.3$ does not produce high-temperature features in the magnetism, in contrast to the $Sr_{2-x}Nd_{1+x}Mn_2O_7$ series. There is no sign of antiferromagnetic order in the 150 K range or the jump in M below 300 K ascribed above to the development of spin clusters. It would seem that increasing the concentration of a lanthanide cation which is too small to support CMR cannot induce a transition to the quasi-delocalised behaviour of the e_g electrons required to produce high-temperature magnetic irreversibility regardless of the concentration of the e_g electrons. The size of the lanthanide would then appear to be critical in controlling the electronic properties. One interpretation is that competition for bonding to oxygen prevents delocalisation of the e_g electrons by narrowing the Mn *3d* bands. The e_g electrons remain localised for all Mn^{III} concentrations in the $Sr_{2-x}Tb_{1+x}Mn_2O_7$ series. The positive Weiss constant for $x=0.5$ suggests increasingly strong t_{2g}–e_g ferromagnetic superexchange coupling as the Mn^{III} concentration is increased.

In the $Sr_{2-x}Nd_{1+x}Mn_2O_7$ series, both synchrotron and laboratory powder X-ray diffraction measurements indicate that these compounds are single phase for $x \geqslant 0.4$[18] This transition corresponds to a change in the qualitative temperature dependence of the magnetisation behaviour, together with generally smaller magnetisations being found for the single-phase materials. We can use the magnetic response to separate the single-phase from the biphasic compositions. $x=0.2$ and 0.3 have similar magnetism to $x=0.0$ and 0.1 with a sharp increase in the magnetisation measured at 0.05 T just below 300 K. The correspondence in electronic properties extends to the existence of CMR, which is also displayed by $x=0.2$.[11] Several problems with simple interpretations of the electronic properties of these systems are posed by the multiphasic nature revealed by powder neutron diffraction for samples with $x=0.0$ and 0.1.[13] Measurement of magnetisation isotherms for several temperatures below the jump temperature, at which the magnetisation rises sharply, reveals saturation moments of 0.54 μ_B/Mn for $x=0.2$ and 0.24 μ_B/Mn for $x=0.1$. The measurements show no evidence for a remanent magnetisation and the coercive field is <0.01 T. It is clear that the jump in the magnetisation which is correlated with this low-field hysteresis is not associated with magnetic long-range order for $x=0.0$ or 0.1. The small saturation moment could only be due to canting of a predominantly antiferromagnetic system and the Bragg peaks would be clearly visible in powder neutron diffraction (as they are below the Neel temperatures of 137 and 100 K for $x=0.0$ and 0.1[13]). Measurements on $Nd_{1.8}Sr_{1.2}Mn_2O_7$ in 0.05 and 1.45 T fields show that this feature is broadened on increasing the measuring field. The jump in the magnetisation and subsequent small hysteresis with small saturation moment is consistent with the blocking of superparamagnetic clusters with a range of volumes: the blocking of successively smaller clusters as the temperature is reduced accounts for the increasing saturation moment and area of the hysteresis loops. This would be consistent with the development of regions of ferromagnetic spin correlation in the vicinity of the Mn^{III} sites, suggestive of the formation of spin polarons or the development of short-range two-dimensional ordering within the bilayers, as previously suggested for the $Sr_{2-x}La_{1+x}Mn_2O_7$ materials above their three-dimensional Curie temperatures.[10,32] It would be reasonable to conclude from the combined similarities of magnetism and magnetotransport of the biphasic $x=0.0$–0.3 materials that for all these samples the two co-existing phases are a blocked superparamagnet/small ferromagnetic cluster phase and an antiferromagnet at low temperatures. It is however important to note that the present measurements cannot distinguish which of the two phases is responsible for the rise in the magnetisation below 300 K. Also, even in the $x=0.0$ and $x=0.1$ cases where antiferromagnetism is apparent in neutron powder diffraction, there is no clear signature of the transition in the magnetisation measurements. The size of the jump suggests that the ferromagnetic clusters are present in their largest concentrations in the $x=0.2$ composition, and the existence of antiferromagnetism for $x \geqslant 0.2$ requires investigation by powder neutron diffraction. The low temperature drop in the 0.05 T ZFC magnetisation of $x=0.2$, for example, may signify the onset of antiferromagnetic order. In contrast to the $La_{1+x}Sr_{2-x}Mn_2O_7$ system, increasing the Mn^{III} concentration from the +3.5 oxidation state does not produce three-dimensional ferromagnetic ordering. The role played by the interfaces between the two phases and possible localised defects in controlling the magnetism of the $Sr_{2-x}Nd_{1+x}Mn_2O_7$ series has yet to be fully understood.

The single-phase samples in the $Sr_{2-x}Nd_{1+x}Mn_2O_7$ series with manganese oxidation states of $<+3.3$ ($x \geqslant 0.4$) differ most obviously in that they do not display such large jumps in their magnetisation below 300 K as found for the biphasic compositions. Inspection of the parameters derived from the high-temperature Curie–Weiss fits to $Sr_{1.6}Nd_{1.4}Mn_2O_7$ and $Sr_{1.3}Nd_{1.7}Mn_2O_7$ show that the Weiss constant is now significant and positive (*ca.* +80 K), while the derived moment is consistently higher than that expected from the non-interacting single ions. The function $\partial(\chi T)/\partial T$ peaks at 200 K ($x=0.4$, 0.5)

and 110 K ($x=0.7$), consistent with transitions involving the manganese sublattice: in the case of $Sr_{1.3}Nd_{1.7}Mn_2O_7$, this temperature coincides with the FC/ZFC divergence in 0.01 T. These observations are all consistent with the occurrence of co-operative magnetism in these materials above the temperature at which the ZFC magnetism reaches its maximum. A divergence between FC and ZFC magnetisation is apparent between 100 and 200 K in a manner associated with slowing of the relaxation dynamics of large volumes of spins within the sample ('blocking of clusters'). Note that the temperature for this irreversible behaviour is higher than that found for the smaller lanthanides. Neutron diffraction measurements are required to evaluate whether the transitions involve the long-range antiferromagnetic ordering or the formation of frozen clusters of spins. At lower temperatures (40–50 K) the temperature dependence of the ZFC magnetisation changes sign; the uncertain influence of the neodymium moments on the FC data makes a clear-cut interpretation impossible, but this behaviour is consistent with spin-glass freezing of some of the moments in the sample. The behaviour of the smaller lanthanide phases suggests that it is the manganese moments which are freezing. However, the transition temperature of *ca.* 40 K in the single-phase Nd samples is similar to that identified by neutron diffraction as the ordering temperature of the rock-salt layer Nd^{3+} cations in one of the phases in $Sr_2NdMn_2O_7$.[13] We therefore cannot rule out the possibility that the manganese moments either freeze or order antiferromagnetically at a higher temperature, and the 40 K feature is associated with the neodymium sublattice.

The irreversible magnetism is best characterised for the $x=0.7$ sample (Fig. 17) where T_F {defined as T [M_{max}(ZFC)]} increases from 45 to 50 K as the measuring field is reduced from 0.05 to 0.01 T, and the cluster blocking is also apparent at higher temperatures in the lower field. The observation of a small hysteresis at 5 K in an $M(H)$ loop is consistent with the assignment of a low-temperature spin-glass phase or with the existence of frozen ferromagnetic clusters. The saturation moment is 0.055 μ_B/Mn. The rise in the FC magnetisation below the freezing temperature is suggestive of the existence of entropic clusters in the predominantly frozen spin system rather than the existence of the uncoupled lanthanide moments observed for the single-phase small lanthanide $Sr_2LnMn_2O_7$ phases. This is because the ZFC magnetisation decreases on cooling below the freezing point. Neutron diffraction shows long range order of the rock-salt layer neodymium moments below 30 K in $Sr_2NdMn_2O_7$[13] and the absence of an increase in the ZFC magnetisation below the freezing temperature suggests that the neodymium moments participate in the spin-glass freezing in the single phase samples too. This is a further contrast with the site-ordered single phase $n=2$ RP materials formed by the smaller lanthanides. The significant lanthanide occupancy of the perovskite block site is a key difference from the more extensively cation-ordered $n=2$ phases found for the smaller lanthanide cations, and the geometric frustration of the Mn–Nd exchange interactions at the perovskite site would prevent these cations from ordering magnetically. This behaviour reinforces the conclusion that the coupling between the lanthanide spins and the manganese spins is strongest for the larger lanthanides where the manganese spins themselves freeze or order at higher temperatures.

$Sr_{1.6}Nd_{1.4}Mn_2O_7$, which is single phase to both laboratory and synchrotron powder X-ray diffraction,[18] may be directly compared to the metallic ferromagnet $La_{1.6}Sr_{1.4}Mn_2O_7$. The lanthanum compound orders ferromagnetically at 90 K in three dimensions but deviates from the Curie–Weiss law below 240 K.[10] This is ascribed to the development of short-range ferromagnetic correlations in two dimensions. In the neodymium case, the Weiss constant and observed magnetic moment are suggestive of predominantly ferromagnetic interactions without ferromagnetic long-range order. One interpretation of the data suggested from the Curie–Weiss fits and the behaviour of $\partial(\chi T)/\partial T$ with temperature is that small clusters with net ferromagnetic moments form below 220 K, block below 130 K and freeze below 45 K. Similar behaviour, with a high-temperature feature in $\partial(\chi T)/\partial T$ followed by FC/ZFC divergence and a maximum in the ZFC magnetisation, is found in the more heavily reduced members of the series.

Colossal magnetoresistance in the Ln = Nd and Pr systems could be associated either with the formation of the small magnetic clusters between 200–300 K or the onset of antiferromagnetic order at lower temperature revealed by powder neutron diffraction. The high-temperature irreversible magnetism and the antiferromagnetic long-range order is suppressed as the Mn oxidation state is reduced towards +III, indicating a similar sensitivity to oxidation state to that found for the three-dimensional perovskites, but without three-dimensional ferromagnetic order driven by delocalisation of the e_g electrons and the concomitant t_{2g}–e_g double exchange interaction. The temperature of the sharp jump in the magnetisation, ascribed to the formation of small ferromagnetic regions, is reduced and the antiferromagnetic long-range order in the vicinity of the +3.5 oxidation state is suppressed as the concentration of electrons in the e_g orbitals increases. These observations are consistent with increasing frustration of the antiferromagnetic interactions which predominate at the +3.5 oxidation state. This in turn suggests that the e_g electrons are responsible for ferromagnetic interactions without being truly delocalised, as there is no evidence for metallic behaviour or three-dimensional ferromagnetism at any point in the series. The positive Weiss constants and enhanced magnetic moments provide support for this view, in which the imperfectly localised e_g spins could be considered as spin polarons, producing small regions of ferromagnetically aligned spins in their vicinity to lower their kinetic energy by increasing the radius over which they are able to hop. The ferromagnetic coupling would then be intermediate in nature between superexchange and true double exchange. In the Tb series, the effect of increased e_g electron concentration on the magnetism is less marked as the reduced e_g bandwidth reduces the radius of the spin polarons and the e_g electrons remain predominantly localised.

We then correlate the much higher conductivities and ferromagnetism of the La phases with the double-exchange interaction produced by e_g electrons which are completely delocalised below the Curie temperature, and assign more localised behaviour to the e_g electrons for all the other lanthanide cations. The differing magnetism can then be attributed to the differences between superexchange and double exchange in competing with the antiferromagnetic t_{2g}–t_{2g} interactions. Arguments for the evolution of the exchange interactions in $n=\infty$ perovskites based on increasing localisation of the e_g electrons are presented in ref. 33.

The $n=2$ systems here which appear to have predominantly localised electrons are, surprisingly, those with the smallest a and c lattice parameters, and therefore the shortest Mn—O and Mn—Mn distances. Detailed crystal structure refinements will allow further comment on the differences in behaviour between the metallic Ln = La and non-metallic Ln = Gd–Er, Y $Sr_2LnMn_2O_7$ samples. In the absence of a powder neutron diffraction study, we may note that the increased Mn–Mn transfer integrals expected on the basis of the decreased Mn—Mn distances will be counteracted by the increasing electronegativity of the smaller lanthanides, which will compete increasing effectively with manganese for bonding with oxygen across the series. The nine-co-ordinate site lanthanide is closer to both the rock-salt layer apical and, more importantly, the equatorial oxygens in the bilayer of MnO_6 octahedra than the twelve-co-ordinate perovskite block cation site,[13] and therefore the effect of the cation ordering will be to accentuate the effect of the smaller lanthanide size on reducing the bandwidth of the Mn-derived electrons. The influence of the increasingly

localised e_g electrons on the t_{2g} Mn–O–Mn antiferromagnetic superexchange is reduced from the dominant ferromagnetic double exchange to a more localised competing ferromagnetic superexchange interaction. A combination of this with the disorder in the system produces spin-glass behaviour.

The current study demonstrates that the transition between the delocalised, ferromagnetic $Sr_{2-x}La_{1+x}Mn_2O_7$ series and the localised spin-glass $Sr_2YMn_2O_7$ which occurs on reducing the size of the lanthanide cation goes *via* the intriguing Nd and Pr systems which show composition-dependent CMR without bulk ferromagnetism. The evolution of the magnetic properties with oxidation state suggests that high-temperature ordering or freezing of the manganese spins is connected with increasing delocalisation of the e_g electrons, in turn governed by the size and electronegativity of the lanthanide cations.

We thank the Donors of the Petroleum Research Foundation, funded by the American Chemical Society, and the EPSRC for support of this work. We thank Dr. P. G. Radaelli (Institut Laue Langevin, Grenoble), Dr. J. Singleton, Dr. S. J. Blundell and Dr. A-K. Klehe (Clarendon Laboratory, Department of Physics, University of Oxford) for their collaboration in this project and for useful discussions. We thank Dr. J. F. Mitchell (Argonne National Laboratory) for communicating results prior to publication, and Dr. S. T. Bramwell (Department of Chemistry, University College, London) for a discussion on two-dimensional ferromagnetism.

References

1 R. von Helmolt, J. Wecker, B. Holzapfel, L. Schultz and K. Samwer, *Phys. Rev. Lett*., 1993, **71**, 2331.
2 S. Jin, T. H. Tiefel, M. McCormack and R. A. Fastnacht, *Science*, 1994, **264**, 413.
3 B. Raveau, A. Maignan and V. Caignaert, *J. Solid State Chem*., 1995, **117**, 424.
4 H. Kamata, Y. Yonemura, J. Mizusaki, H. Tagawa, K. Naraya and T. Sasamoto, *J. Phys. Chem. Solids*, 1995, **56**, 943.
5 Y. Tomioka, A. Asamitsu, H. Kuwahara, Y. Moritomo and Y. Tokura, *Phys. Rev. B*, 1996, **53**, 1689.
6 H. Kuwahara, Y. Tomioka, Y. Moritomo, A. Asamitsu, M. Kasai, R. Kumai and Y. Tokura, *Science*, 1996, **272**, 80.
7 Y. Moritomo, Y. Tomioka, A. Asamitsu and Y. Tokura, *Phys. Rev. B*, 1995, **51**, 3297.
8 Y. Moritomo, A. Asamitsu, H. Kuwahara and Y. Tokura, *Nature* (*London*), 1996, **380**, 141.
9 J. F. Mitchell, D. N. Argyriou, J. D. Jorgensen, D. G. Hinks, C. P. Potter and S. D. Bader, *Phys. Rev. B*, 1997, **55**, 63.
10 T. Kimura, Y. Tomioka, H. Kuwahara, A. Asamitsu, M. Tamura and Y. Tokura, *Science*, 1996, **264**, 1698.
11 P. D. Battle, S. J. Blundell, M. A. Green, W. Hayes, M. Honold, A. K. Klehe, N. S. Laskey, J. E. Millburn, L. Murphy, M. J. Rosseinsky, N. A. Samarin, J. Singleton, N. E. Sluchanko, S. P. Sullivan and J. F. Vente, *J. Phys.: Condens. Matter*, 1996, **8**, L427.
12 R. Seshadri, C. Martin, A. Maignan, M. Hervieu, B. Raveau and C. N. R. Rao, *J. Mater. Chem*., 1996, **6**, 1585.
13 P. D. Battle, M. A. Green, N. S. Laskey, J. E. Millburn, P. G. Radaelli, M. J. Rosseinsky, S. P. Sullivan and J. F. Vente, *Phys. Rev. B*, 1996, **54**, 15967.
14 H. Y. Hwang, S. W. Cheong, N. P. Ong and B. Batlogg, *Phys. Rev. Lett*., 1996, **77**, 2041.
15 J. M. de Teresa, M. R. Ibarra, J. Garcia, J. Blasco, C. Ritter, P. A. Algarabel, C. Marquina and A. del Moral, *Phys. Rev. Lett*., 1996, **76**, 3392.
16 J. Blasco, J. Garcia, J. M. de Teresa, M. R. Ibarra, P. A. Algarabel and C. Marquina, *J. Phys.: Condens. Matter*, 1996, **8**, 7427.
17 P. D. Battle, M. A. Green, N. S. Laskey, J. E. Millburn, L. E. Murphy, M. J. Rosseinsky, S. P. Sullivan and J. F. Vente, *Chem. Mater*., 1997, **9**, 552.
18 P. D. Battle, S. J. Blundell, D. E. Cox, M. A. Green, J. E. Millburn, P. G. Radaelli, M. J. Rosseinsky, L. E. Spring, J. Singleton and J. F. Vente, *Mater. Res. Soc. Proc*., 1996, in the press.
19 P. Schiffer, A. P. Ramirez, W. Bao and S. W. Cheong, *Phys. Rev. Lett*., 1995, **75**, 3336.
20 J. A. M. Vanroosmalen and E. H. P. Cordfunke, *J. Solid State Chem*., 1991, **93**, 212.
21 D. L. Leslie-Pelecky and R. D. Rieke, *Chem. Mater*., 1996, **8**, 1770.
22 J. B. A. A. Elemans, B. van Laar, K. R. van der Veen and B. O. Loopstra, *J. Solid State Chem*., 1971, **3**, 238.
23 S. Satpathy, Z. S. Popovic and F. R. Vukajlovic, *Phys. Rev. Lett*., 1996, **76**, 960.
24 J. H. Park, C. T. Chen, S. W. Cheong, W. Bao, G. Meigs, V. Chakarian and Y. U. Idzerda, *Phys. Rev. Lett*., 1996, **76**, 4215.
25 P. D. Battle, S. J. Blundell, M. A. Green, A. K. Klehe, J. E. Millburn, J. Singleton, L. E. Spring and J. F. Vente, unpublished work.
26 A. Urushibara, Y. Moritomo, T. Arima, A. Asamitsu, G. Kido and Y. Tokura, *Phys. Rev. B*, 1995, **51**, 14103.
27 W. Bao, C. H. Chen, S. A. Carter and S. W. Cheong, *Solid State Commun*, 1996, **98**, 55.
28 P. G. Radaelli, D. E. Cox, M. Marezio, S. W. Cheong, P. E. Schiffer and A. P. Ramirez, *Phys. Rev. Lett*., 1995, **75**, 4488.
29 J. Fontcuberta, B. Martinez, A. Seffar, S. Pinol, J. L. Garcia-Munoz and X. Obradors, *Europhys. Lett*., 1996, **34**, 379.
30 P. D. Battle, P. G. Radaelli, M. J. Rosseinsky, L. E. Spring and J. F. Vente, unpublished work.
31 P. D. Battle, D. E. Cox, M. A. Green, J. E. Millburn, P. G. Radaelli, M. J. Rosseinsky and L. E. Spring, *Chem. Mater*., in press.
32 J. F. Mitchell, personal communication.
33 J. M. D. Coey, M. Viret, L. Ranno and K. Ounadjela, *Phys. Rev. Lett*., 1995, **75**, 3910.

Paper 6/08501F; *Received* 19*th December*, 1996